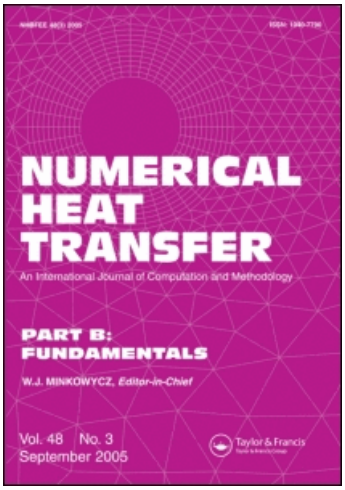

Numerical Heat Transfer, Part B: Fundamentals
Publication details, including instructions for authors and subscription information:
http://www.informaworld.com/smpp/title~content=t713723316

Performance Analysis of IDEAL Algorithm Combined with Bi-CGSTAB Method

D. L. Sun [a]; Y. P. Yang [a]; J. L. Xu [a]; W. Q. Tao [b]
[a] Beijing Key Laboratory of New and Renewable Energy, North China Electric Power University, Beijing, People's Republic of China [b] School of Energy & Power Engineering, Xi'an Jiaotong University, Xi'an, Shaanxi, People's Republic of China

Online publication date: 11 January 2010

To cite this Article Sun, D. L., Yang, Y. P., Xu, J. L. and Tao, W. Q.(2009) 'Performance Analysis of IDEAL Algorithm Combined with Bi-CGSTAB Method', Numerical Heat Transfer, Part B: Fundamentals, 56: 6, 411 — 431
To link to this Article: DOI: 10.1080/10407790903526725
URL: http://dx.doi.org/10.1080/10407790903526725

Numerical Heat Transfer, Part B, 56: 411–431, 2009

ISSN: 1040-7790 print/1521-0626 online
DOI: 10.1080/10407790903526725

Taylor & Francis
Taylor & Francis Group

PERFORMANCE ANALYSIS OF IDEAL ALGORITHM COMBINED WITH Bi-CGSTAB METHOD

D. L. Sun[1], Y. P. Yang[1], J. L. Xu[1], and W. Q. Tao[2]

[1]*Beijing Key Laboratory of New and Renewable Energy, North China Electric Power University, Beijing, People's Republic of China*

[2]*School of Energy & Power Engineering, Xi'an Jiaotong University, Xi'an, Shaanxi, People's Republic of China*

An efficient segregated algorithm for fluid flow and heat transfer problems, called IDEAL, was proposed D. L. Sun et al. [11]. In addition, the IDEAL algorithm was extended to 2-Dl 3-D grid systems. In these IDEAL algorithms, all of the algebraic equations are solved by the alternating-direction implicit (ADI) method, called the IDEAL+ADI method. In this article, the efficient Bi-CGSTAB method is adopted instead of the ADI method to solve the algebraic equations in the IDEAL algorithm, called the IDEAL+Bi-CGSTAB method. It is found that the IDEAL+Bi-CGSTAB method is much better than the IDEAL+ADI method to solve open systems but little worse to solve closed systems.

1. INTRODUCTION

Numerical approaches to solve the Navier-Stokes equations can be divided into two categories [1, 2]: density-based and pressure-based. The pressure-based approach, or the primitive-variables approach, was originally developed for solving incompressible fluid flows, but it has been successfully extended to compressible flows. It has been widely used in computational fluid flow and heat transfer problems. Among the pressure-based approaches, the pressure-correction method is the most widely used one because of its simplicity and straightforward physical mechanism point of view. The first pressure-correction method was the SIMPLE algorithm, proposed by Patankar and Spalding in 1972 [3]. The major approximations made in the SIMPLE algorithm are that (1) the initial pressure field and velocity field are assumed independently, thus the coupling between pressure and velocity is neglected; and (2) effect of the velocity corrections of the neighboring grids is not considered to simplify the solution procedure, leading to the semi-implicit nature of the algorithm. The two approximations do not influence the final solutions if the

Received 27 October 2009; accepted 27 November 2009.

This work was supported by the Key Project of the National Natural Science Foundation of China (50636050), the National Natural Science Foundation of China (No. 50825603), and the National Key Project for R&D of China (2009CB219801).

Address correspondence to Y. P. Yang, Beijing Key Laboratory of New and Renewable Energy, North China Electric Power University, Beijing 102206, People's Republic of China. E-mail: yyp@ncepu.edu.cn

NOMENCLATURE

a	coefficient in the discretized equation	Γ	nominal diffusion coefficient
A	surface area, nonzero diagonal	η	dynamic viscosity
$\underline{A}$	coefficient matrix	ν	kinematic viscosity
$\overline{b}$	constant term in the discretized equation	ρ	density
d	coefficient in the velocity-correction equation	ϕ	general variable
E	time-step multiple	**Subscripts**	
N1, N2	inner doubly iterative times	e, w, n, s, t, b	cell surface
p	pressure	in	inlet
q_m	reference mass flow rate	nb	neighboring grid points
Re	Reynolds number	P, E, N, S, W, T, B	grid point
$\mathrm{Rs}_{\mathrm{Mass}}$	relative maximum mass residual	u, v, w	referring to u, v, w momentum equation
$\mathrm{Rs}_{U\mathrm{Mom}}$, $\mathrm{Rs}_{V\mathrm{Mom}}$, $\mathrm{Rs}_{W\mathrm{Mom}}$	relative maximum u-, v-, w-component momentum residuals	ϕ	general variable
		Superscripts	
S	source term	PTemp	temporary value in previous inner iteration step
T	temperature	Temp	temporary value in current inner iteration step
u, v, w	velocity component in x, y, z directions	0	previous iteration
$\tilde{u}$, $\tilde{v}$, $\tilde{w}$	pseudo-velocity	$*$	intermediate value in iteration
x, y, z	coordinates	$'$	correction
α	underrelaxation factor		

solution process is converged [4], but they affect the convergence rate and stability of the solution. Therefore, since the development of the SIMPLE algorithm, a number of modified methods, such as SIMPLER [5], SIMPLEC [6], SIMPLEX [7], PISO [8], CLEAR [9, 10], etc., have been proposed in order to overcome one or both of the approximations. Unlike other algorithms, in order to obtain an incompressible flow field which satisfies the mass conservation law, the CLEAR algorithm does not introduce a pressure correction. The algorithm improves the intermediate velocity by solving a pressure equation to make the algorithm fully implicit, since no term is omitted in the derivation process. However, the robustness of the CLEAR algorithm is somewhat weakened by solving the pressure equation directly. To overcome this disadvantage, the IDEAL algorithm (Inner Doubly iterative Efficient Algorithm for Linked equations) was proposed in [11, 12]. In this algorithm there exist inner doubly iterative processes for the pressure equation at each iteration level, which almost completely resolves the two approximations in the SIMPLE algorithm. Thus the coupling between velocity and pressure is fully guaranteed, greatly enhancing the convergence rate and stability of the solution process. Recently, the IDEAL algorithm was extended to the staggered grid system [13] and the collocated grid system in 3-D Cartesian coordinates [14].

In these IDEAL algorithms, all of the algebraic equations, formed by discretizing governing equations, were solved by the alternative-direction implicit (ADI) method [15], called the IDEAL+ADI method. The ADI method needs less computing memory but has low solution speed. Because it uses less computer resources, the ADI method has been widely used. With the development of the computer industry,

more efficient methods for solving algebraic equations are needed. Krylov subspace methods [16], representing an advanced technique for solving algebraic equations, have been the most important iteration technique for solving large linear systems because of its fast solution speed. Krylov subspace methods include methods such as Bi-CGSTAB [17, 18], GMRES(m) [19], CGS [20], TFQMR [21], QMR [22], etc., which were compared with each other in [23]. It was found that the Bi-CGSTAB method is much more stable and more efficient among all the methods. In this articles, the Bi-CGSTAB method is used instead of the ADI method to solve the algebraic equations in the IDEAL algorithm.

For linear problems, the algebraic equations are solved only once, so the solution speed by the Bi-CGSTAB method is about 50 times faster than that by the ADI method. The advantage of the Bi-CGSTAB method over the ADI method is verified by simulating a 3-D heat conduction problem. The governing equation and the boundary conditions for the problem studied are as follows:

$$\begin{aligned} &\frac{\partial^2 T}{\partial x^2}+\frac{\partial^2 T}{\partial y^2}+\frac{\partial^2 T}{\partial z^2}=0 \quad (0<x<10, 0<y<10, 0<z<10)\\ &T(0,y,z)=0 \qquad T(10,y,z)=0\\ &\partial T(x,0,z)/\partial y=0 \qquad \partial T(x,10,z)/\partial y=0\\ &T(x,y,0)=0 \qquad T(x,y,10)=100 \end{aligned} \tag{1}$$

Equation (1) is solved analytically [24] and by the numerical schemes ADI and Bi-CGSTAB. The grid number $80 \times 80 \times 80$ is included in the numerical simulations. Figure 1 shows the computed temperature at the plane $y=5$ using different methods. It is found that the temperature fields simulated by the ADI and Bi-CGSTAB methods agree very well with that by the analytical solution, proving the validity of the ADI and Bi-CGSTAB methods. For this specific problem, the solution speed by the Bi-CGSTAB method is 40 times faster than that by the ADI method, showing the advantage of the Bi-CGSTAB method for the linear heat transfer problem studied.

For nonlinear fluid flow and heat transfer problems, the simulation is performed by iteration. At each iteration step, the algebraic equations are solved with updated coefficients. The solution is the intermediate temporary value. Thus

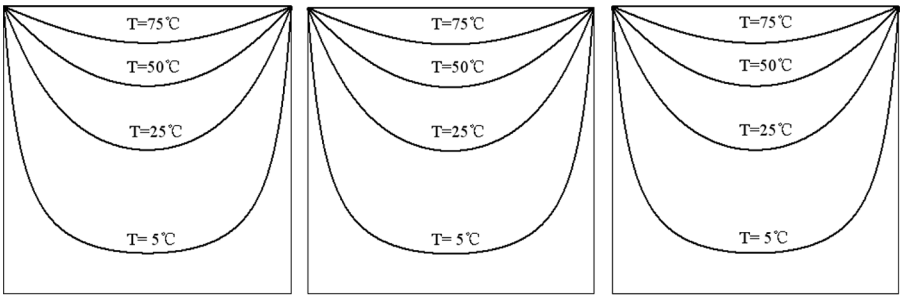

(*a*) Analysis method (*b*) ADI method (*c*) Bi-CGSTAB method

Figure 1. Temperature at the plane $y=5$ calculated by different methods.

the convergence rate of nonlinear problems depends on both the solution speed of the algebraic equations and the stability of the iteration process. It is not certain that the Bi-CGSTAB method is superior to the ADI method for nonlinear problems. The objective of the present article is to verify the effectiveness of the Bi-CGSTAB method. Four nonlinear fluid flow problems, two for open systems and two for closed systems, are simulated by the IDEAL+Bi-CGSTAB method and the IDEAL+ADI method using a 3-D staggered grid system.

This article is organized as follows. The governing equations and their discretization forms are described first. The major solution procedures of the IDEAL algorithm and the ADI/Bi-CGSTAB methods are briefly reviewed. A systemic comparison between the IDEAL+ADI method and the IDEAL+Bi-CGSTAB method is performed, focusing on the robustness and convergence rate of these numerical schemes. The major conclusions are summarized at the end of the article.

2. GOVERNING EQUATIONS

We gave the governing equations and their discretization forms. An incompressible steady laminar flow in 3-D Cartesian coordinates is taken as an example. The governing equations are written as follows.

Continuity equation:

$$\frac{\partial(\rho u)}{\partial x}+\frac{\partial(\rho v)}{\partial y}+\frac{\partial(\rho w)}{\partial z}=0 \tag{2}$$

Momentum equation:

$$\frac{\partial(\rho uu)}{\partial x}+\frac{\partial(\rho vu)}{\partial y}+\frac{\partial(\rho wu)}{\partial z}=-\frac{\partial p}{\partial x}+\eta\left(\frac{\partial^2 u}{\partial x^2}+\frac{\partial^2 u}{\partial y^2}+\frac{\partial^2 u}{\partial z^2}\right)+S_u \tag{3}$$

$$\frac{\partial(\rho uv)}{\partial x}+\frac{\partial(\rho vv)}{\partial y}+\frac{\partial(\rho wv)}{\partial z}=-\frac{\partial p}{\partial y}+\eta\left(\frac{\partial^2 v}{\partial x^2}+\frac{\partial^2 v}{\partial y^2}+\frac{\partial^2 v}{\partial z^2}\right)+S_v \tag{4}$$

$$\frac{\partial(\rho uw)}{\partial x}+\frac{\partial(\rho vw)}{\partial y}+\frac{\partial(\rho ww)}{\partial z}=-\frac{\partial p}{\partial z}+\eta\left(\frac{\partial^2 w}{\partial x^2}+\frac{\partial^2 w}{\partial y^2}+\frac{\partial^2 w}{\partial z^2}\right)+S_w \tag{5}$$

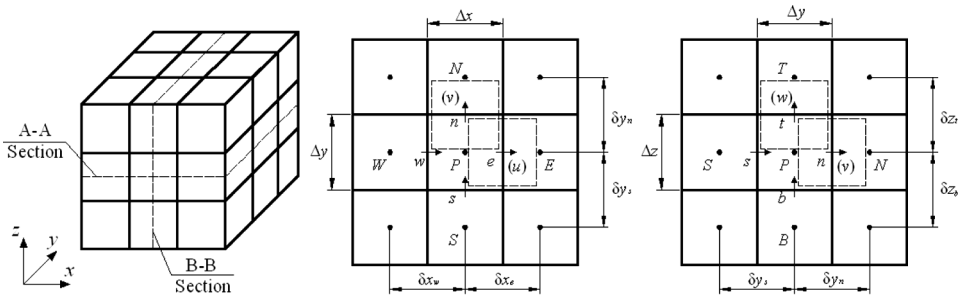

(*a*) 3-D grid system (*b*) A-A section (*c*) B-B section

Figure 2. Control volumes on a staggered grid system in 3-D Cartesian coordinates.

The finite-volume method (FVM) [4, 25] is used to discretize the continuity and momentum equations on the staggered grid system, which is shown in Figure 2.

The discretized continuity equation is

$$(\rho u)_e A_e - (\rho u)_w A_w + (\rho v)_n A_n - (\rho v)_s A_s + (\rho w)_t A_t - (\rho w)_b A_b = 0 \tag{6}$$

The discretized momentum equation is

$$\frac{a_e}{\alpha_u} u_e = \sum a_{\mathrm{nb}} u_{\mathrm{nb}} + b_e + d_e(p_P - p_E) \tag{7}$$

$$\frac{a_n}{\alpha_v} v_n = \sum a_{\mathrm{nb}} v_{\mathrm{nb}} + b_n + d_n(p_P - p_N) \tag{8}$$

$$\frac{a_t}{\alpha_w} w_t = \sum a_{\mathrm{nb}} w_{\mathrm{nb}} + b_t + d_t(p_P - p_T) \tag{9}$$

where the underrelaxation factor α is incorporated into the solution process of the algebraic equations. The terms $(1-\alpha_u)a_e u_e^0/\alpha_u$, $(1-\alpha_v)a_n v_n^0/\alpha_v$, and $(1-\alpha_w)a_t w_t^0/\alpha_w$ are incorporated into the source terms b_e, b_n, and b_t, respectively. The coefficients a and source terms b depend on the discretized schemes, which are well documented in [4, 25, 26], and are thus not repeated here.

3. SOLUTION PROCEDURE OF THE IDEAL ALGORITHM

The IDEAL algorithm was proposed for incompressible fluid flow and heat transfer problems using the staggered grid system in 3-D Cartesian coordinates in [13]. The major points of the IDEAL algorithm are reviewed here. Figure 3

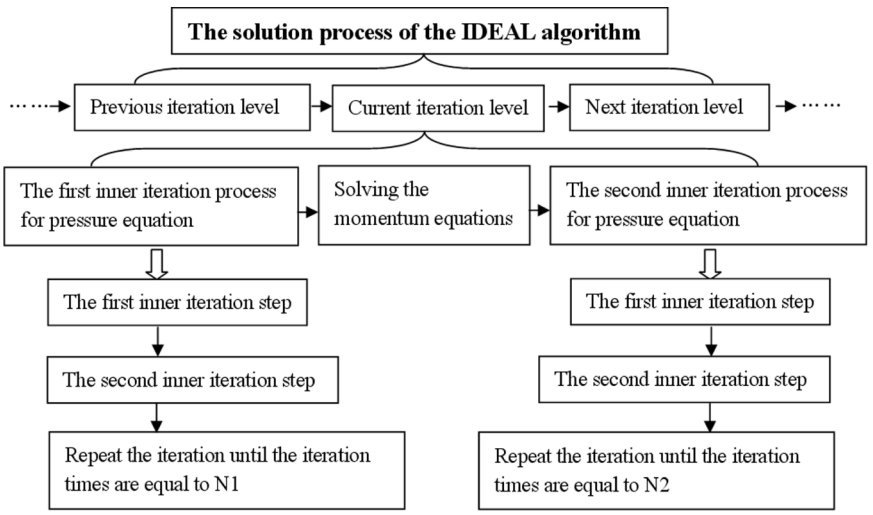

Figure 3. Framework of the solution process of the IDEAL algorithm.

shows the detailed framework of the IDEAL algorithm, which is summarized as follows.

Step 1. Assume an initial velocity field u^0, v^0, and w^0.

Step 2. Calculate the coefficients a and source terms b of the discretized momentum equations (7)–(9), using the initial velocity field.

First inner iteration process for pressure question.

Step 3. Calculate the pseudo-velocities $\tilde{u}^0$, $\tilde{v}^0$, and $\tilde{w}^0$ defined in Eqs. (10)–(12).

$$u_e^{\text{Temp}} = \frac{\sum a_{\text{nb}} u_{\text{nb}}^0 + b_e}{a_e/\alpha_u} + d_e\left(p_P^{\text{Temp}} - p_E^{\text{Temp}}\right) = \tilde{u}_e^0 + d_e\left(p_P^{\text{Temp}} - p_E^{\text{Temp}}\right) \tag{10}$$

$$v_n^{\text{Temp}} = \frac{\sum a_{\text{nb}} v_{\text{nb}}^0 + b_n}{a_n/\alpha_v} + d_n\left(p_P^{\text{Temp}} - p_N^{\text{Temp}}\right) = \tilde{v}_n^0 + d_n\left(p_P^{\text{Temp}} - p_N^{\text{Temp}}\right) \tag{11}$$

$$w_t^{\text{Temp}} = \frac{\sum a_{\text{nb}} w_{\text{nb}}^0 + b_t}{a_t/\alpha_w} + d_t\left(p_P^{\text{Temp}} - p_T^{\text{Temp}}\right) = \tilde{w}_t^0 + d_t\left(p_P^{\text{Temp}} - p_T^{\text{Temp}}\right) \tag{12}$$

Step 4. Solve the pressure equation (13), and obtain the temporary pressure p^{Temp}.

$$\begin{aligned}
&\frac{a_P}{\alpha_p} p_P^{\text{Temp}} = \sum a_{\text{nb}} p_{\text{nb}}^{\text{Temp}} + b \\
&a_P = a_E + a_W + a_N + a_S + a_T + a_B \\
&a_E = (\rho A d)_e, \quad a_W = (\rho A d)_w, \quad a_N = (\rho A d)_n \\
&a_S = (\rho A d)_s, \quad a_T = (\rho A d)_t, \quad a_B = (\rho A d)_b \\
&b = (\rho \tilde{u}^0 A)_w - (\rho \tilde{u}^0 A)_e + (\rho \tilde{v}^0 A)_s - (\rho \tilde{v}^0 A)_n + (\rho \tilde{w}^0 A)_b - (\rho \tilde{w}^0 A)_t \\
&\qquad + (1 - \alpha_p)\frac{a_P}{\alpha_p} p_P^{P\text{Temp}}
\end{aligned} \tag{13}$$

Equation (13) is obtained by substituting Eqs. (10)–(12) into the discretized continuity equation (6).

Step 5. Calculate the temporary velocities u^{Temp}, v^{Temp}, and w^{Temp} from Eqs. (10)–(12) by the temporary pressure p^{Temp}. Then the first inner iteration step is completed and the next inner iteration step starts.

Step 6. Record u^{Temp}, v^{Temp}, w^{Temp}, and p^{Temp}, which are calculated in steps 4 and 5, as the temporary velocity and pressure of the previous inner iteration step (u^{PTemp}, v^{PTemp}, w^{PTemp}, and p^{PTemp}). Return to step 3, in which all the superscripts 0 in steps 3 and 4 are replaced by PTemp. Thus the values of $\tilde{u}^0$, $\tilde{v}^0$, and $\tilde{w}^0$ are updated. Then the pressure equation (13) is resolved. Repeat the iteration process, including steps 3, 4, and 5, until the iteration times equals to the prespecified value of N1. Once the first inner iteration process for the pressure equation is completed, the final temporary pressure p^{Temp} is treated as the initial pressure p^*.

Step 7. Solve the discretized momentum equations (7)–(9) by the initial velocity and pressure p^*, and obtain the intermediate velocities u^*, v^*, and w^*.

Second inner iteration process for pressure question.

Step 8. Calculate the pseudo-velocities $\tilde{u}^*$, $\tilde{v}^*$, and $\tilde{w}^*$ defined in Eqs. (14)–(16).

$$u_e^{\text{Temp}} = \frac{\sum a_{\text{nb}} u_{\text{nb}}^* + b_e}{a_e/\alpha_u} + d_e(p_P^{\text{Temp}} - p_E^{\text{Temp}}) = \tilde{u}_e^* + d_e(p_P^{\text{Temp}} - p_E^{\text{Temp}}) \quad (14)$$

$$v_n^{\text{Temp}} = \frac{\sum a_{\text{nb}} v_{\text{nb}}^* + b_n}{a_n/\alpha_v} + d_n(p_P^{\text{Temp}} - p_N^{\text{Temp}}) = \tilde{v}_n^* + d_n(p_P^{\text{Temp}} - p_N^{\text{Temp}}) \quad (15)$$

$$w_t^{\text{Temp}} = \frac{\sum a_{\text{nb}} w_{\text{nb}}^* + b_t}{a_t/\alpha_w} + d_t(p_P^{\text{Temp}} - p_T^{\text{Temp}}) = \tilde{w}_t^* + d_t(p_P^{\text{Temp}} - p_T^{\text{Temp}}) \quad (16)$$

Step 9. Solve the pressure equation (17), and obtain the temporary pressure p^{Temp}.

$$\begin{aligned} &a_P p_P^{\text{Temp}} = \sum a_{\text{nb}} p_{\text{nb}}^{\text{Temp}} + b \\ &a_P = a_E + a_W + a_N + a_S + a_T + a_B \\ &a_E = (\rho A d)_e, \quad a_W = (\rho A d)_w, \quad a_N = (\rho A d)_n \\ &a_S = (\rho A d)_s, \quad a_T = (\rho A d)_t, \quad a_B = (\rho A d)_b \\ &b = (\rho \tilde{u}^* A)_w - (\rho \tilde{u}^* A)_e + (\rho \tilde{v}^* A)_s - (\rho \tilde{v}^* A)_n + (\rho \tilde{w}^* A)_b - (\rho \tilde{w}^* A)_t \end{aligned} \quad (17)$$

Step 10. Calculate the temporary velocities u^{Temp}, v^{Temp}, and w^{Temp} from Eqs. (14)–(16) by the temporary pressure p^{Temp}. Then an inner iteration step is finished and the next inner iteration step begins.

Step 11. Regard u^{Temp}, v^{Temp}, w^{Temp}, and p^{Temp} calculated in steps 9 and 10 as the temporary velocity and pressure of the previous inner iteration step, denoted by u^{PTemp}, v^{PTemp}, w^{PTemp}, and p^{PTemp}. Return to step 8. All the superscripts * in steps 8 and 9 are replaced by PTemp, thus the values of $\tilde{u}^*$, $\tilde{v}^*$, and $\tilde{w}^*$ are updated. Resolve the pressure equation (17). Repeat the iteration, including steps 8, 9, and 10, until the iteration times equals the prespecified value N2. Once the second inner iteration process for the pressure equation is finished, the final temporary velocities u^{Temp}, v^{Temp}, and w^{Temp} are taken as the final velocities u, v, and w of the current iteration level.

Step 12. Regard the final velocities u, v, and w as the initial velocities u^0, v^0, and w^0 of the next iteration level, then return to step 2 for the next iteration level. Repeat the iterative procedure until convergence is reached.

In the IDEAL algorithm, the first inner iteration times N1 and the second inner iteration times N2 can be adjusted. N1 and N2 should be increased with an increase of the velocity underrelaxation factor.

4. THE ADI AND BI-CGSTAB METHODS

During the solution process in the IDEAL algorithm, all the algebraic equations, including the discretized pressure equation (13) in step 4, the discretized momentum equations (7)–(9) in step 7, and the discretized pressure equation (17) in step 9, will be solved. The general expression form of these discretized

equations (7)–(9), (13), and (17) is written as

$$a_P\phi_P = a_E\phi_E + a_W\phi_W + a_N\phi_N + a_S\phi_S + a_T\phi_T + a_B\phi_B + b \tag{18}$$

The matrix form is

$$\underline{A}\vec{\phi} = \vec{B} \tag{19}$$

where the matrix $\underline{A}$ is expressed as

$$\underline{A} = \begin{pmatrix} A^P & A^E & 0 & \cdots & 0 & A^T \\ A^W & A^P & A^E & 0 & \cdots & 0 \\ 0 & \ddots & \ddots & \ddots & \ddots & \vdots \\ \vdots & \ddots & \ddots & \ddots & \ddots & 0 \\ 0 & \cdots & 0 & A^W & A^P & A^E \\ A^N & 0 & \cdots & 0 & A^W & A^P \end{pmatrix}$$

In Eq. (20), the seven nonzero diagonals A^P, A^E, A^W, A^N, A^S, A^T, and A^B consist of the coefficients a_P, $-a_E$, $-a_W$, $-a_N$, $-a_S$, $-a_T$, and $-a_B$.

The algebraic equations will be solved using the two methods, ADI and Bi-CGSTAB, which are described as follows.

4.1. The ADI Method

The alternative-direction implicit (ADI) method is one of the line-by-line methods. One round of iteration of the ADI method to solve Eq. (18) consists of the following three steps.

Step 1. Solve ϕ along the x coordinate by the tridiagonal matrix algorithm (TDMA) method [25], which is performed for all the x coordinates.

$$a_P\phi_P^{n+1/3} = a_E\phi_E^{n+1/3} + a_W\phi_W^{n+1/3} + (a_N\phi_N^n + a_S\phi_S^n + a_T\phi_T^n + a_B\phi_B^n + b) \tag{21}$$

Step 2. Solve ϕ along the y coordinate, which is performed for all the y coordinates.

$$\begin{aligned} a_P\phi_P^{n+2/3} = {} & a_N\phi_N^{n+2/3} + a_S\phi_S^{n+2/3} + (a_E\phi_E^{n+1/3} + a_W\phi_W^{n+1/3} + a_T\phi_T^{n+1/3} \\ & + a_B\phi_B^{n+1/3} + b) \end{aligned} \tag{22}$$

Step 3. Solve ϕ along the z coordinate, which is performed for all the z coordinates.

$$a_P\phi_P^{n+1} = a_T\phi_T^{n+1} + a_B\phi_B^{n+1} + (a_E\phi_E^{n+2/3} + a_W\phi_W^{n+2/3} + a_N\phi_N^{n+2/3} + a_S\phi_S^{n+2/3} + b) \tag{23}$$

4.2. The Bi-CGSTAB Method

The seven nonzero diagonals of matrix $\underline{A}$ in Eq. (20) are written as

$$\text{entry}(\underline{A}) = (A^B, A^S, A^W, A^P, A^E, A^N, A^T) \tag{24}$$

where the seven entries represent the elements occupying the seven nonzero diagonals of the original coefficient matrix $\underline{A}$.

We use the MILU method [27] to precondition the matrix $\underline{A}$. The preconditioner $\underline{M}$ is defined as

$$\underline{M} = \underline{L}\underline{D}\underline{U} \tag{25}$$

The matrix entries of $\underline{L}$, $\underline{D}$, and $\underline{U}$ are written as

$$\begin{aligned}
\text{entry}(\underline{L}) &= \left(A^{\mathrm{S}},\ A^{\mathrm{W}},\ \frac{1}{D^{\mathrm{P}}},\ 0,\ 0\right) \\
\text{entry}(\underline{D}) &= (0,\ 0, D^{\mathrm{P}}, 0,\ 0) \\
\text{entry}(\underline{U}) &= \left(0,\ 0, \frac{1}{D^{\mathrm{P}}}, A^{\mathrm{E}},\ A^{\mathrm{N}}\right)
\end{aligned} \tag{26}$$

where D^P is computed as

$$D^{\mathrm{P}}_{I,J} = \frac{1}{A^{\mathrm{P}}_{I,J} - D^{\mathrm{P}}_{I-1,J} A^{\mathrm{W}}_{I,J}(A^{\mathrm{E}}_{I-1,J} + \alpha A^{\mathrm{N}}_{I-1,J}) - D^{\mathrm{P}}_{I,J-1} A^{\mathrm{S}}_{I,J}(A^{\mathrm{N}}_{I,J-1} + \alpha A^{\mathrm{E}}_{I,J-1})} \tag{27}$$

where α is set to be 0.99.

Based on the preconditioner $\underline{M}$, the procedure of the Bi-CGSTAB method to solve Eq. (19) is as follows.

Step 1. $\overrightarrow{\phi^0}$ is an initial vector; $\overrightarrow{r^0} = \vec{B} - \underline{A}\,\overrightarrow{\phi^0}$.

Step 2. $\overrightarrow{r'}$ is an arbitrary vector, such that $(\overrightarrow{r'}, \overrightarrow{r^0}) \neq 0$, e.g., $\overrightarrow{r'} = \overrightarrow{r^0}$; $\rho^0 = \alpha = \omega^0 = 1$; $\overrightarrow{v^0} = \overrightarrow{p^0} = 0$.

Step 3. For $n = 1, 2, \ldots$ until $\overrightarrow{r^n} <$ tolerance, $\rho^n = (\overrightarrow{r'}, \overrightarrow{r^{n-1}})$; $\beta = (\rho^n/\rho^{n-1})/(\alpha/\omega^{n-1})$; $\overrightarrow{p^n} = \overrightarrow{r^{n-1}} + \beta(\overrightarrow{p^{n-1}} - \omega^{n-1}\overrightarrow{v^{n-1}})$.

Solve $\vec{y}$ from $\underline{M}\vec{y} = \overrightarrow{p^n}$; $\overrightarrow{v^n} = \underline{A}\vec{y}$; $\alpha = \rho^n/(\overrightarrow{r'}, \overrightarrow{v^n})$; $\vec{s} = \overrightarrow{r^{n-1}} - \alpha\overrightarrow{v^n}$.

Solve $\vec{z}$ from $\underline{M}\vec{z} = \vec{s}$; $\vec{t} = \underline{A}\vec{z}$; $\vec{t} = \underline{A}\vec{z}$; $\omega^n = (\vec{t}, \vec{s})/(\vec{t}, \vec{t})$.

Then the new vector is $\overrightarrow{\phi^n} = \overrightarrow{\phi^{n-1}} + \alpha\overrightarrow{y} + \omega^n\vec{z}$; $\overrightarrow{r^n} = \vec{s} - \omega^n\vec{t}$.

5. COMPARISON CONDITIONS AND CONVERGENCE CRITERIA

In order to perform effective comparisons between the IDEAL+ADI and IDEAL+Bi-CGSTAB methods, numerical simulation conditions and convergence criteria should be specified, which are described as follows.

Hardware and software. All the simulations are performed using a computer with a 2.51-GHz CPU with 2.0 GB RAM along with a FORTRAN 77 compiler.

Discretization scheme. In order to guarantee the stability and accuracy of the numerical solution, the SGSD scheme [28] is adopted, which is at least of

second-order accuracy and absolutely stable. The deferred-correction method is adopted to ensure the stability of the computations, which was proposed in [29] and latter improved in [30].

Iteration times of the ADI and Bi-CGSTAB methods. For nonlinear fluid flow and heat transfer problems, the iteration process was performed. At each iteration level, the algebraic equations with updated coefficients should be solved, and the solution is only the intermediate temporary value in the iteration process. So it is not necessary to reach a convergent solution at each iteration level. Therefore, both the iteration times of the ADI method and the Bi-CGSTAB method are set to be 1.

Underrelaxation factor. In the IDEAL algorithm the underrelaxation factor α_P for pressure is set to be unity, and the underrelaxation factors are the same for the three velocity components of u, v, w, i.e., $\alpha_u = \alpha_v = \alpha_w$. The time-step multiple E is defined in Eq. (28) as

$$E = \frac{\alpha_{u,v,w}}{1 - \alpha_{u,v,w}} \qquad (0 < \alpha_{u,v,w} < 1) \tag{28}$$

The relationship between $\alpha_{u,v,w}$ and E is shown in Table 1. It is seen that the range of the time-step multiple is significantly enlarged using Eq. (28). E approaches infinity when the underrelaxation factor approaches unity.

Grid system. The same uniform grid system is used for both the IDEAL+ ADI method and the IDEAL+Bi-CGSTAB method, which will be shown later.

Convergence criteria. The convergence criteria require that both the relative maximum residuals of mass and momentum with respect to the three velocity components of u, v, w are less than the prespecified values.

The relative maximum mass residual is expressed as

$$\mathrm{Rs}_{\mathrm{Mass}} = \frac{\mathrm{MAX}\left[\left|(\rho u^* A)_w - (\rho u^* A)_e + (\rho v^* A)_s - (\rho v^* A)_n + (\rho w^* A)_b - (\rho w^* A)_t\right|\right]}{q_m} \tag{29}$$

where u^*, v^*, and w^* are the intermediate velocities at each iteration level and q_m is the reference mass flow rate. For open systems, the inlet mass flow rate is treated as the reference value. For closed systems, the mass flow rate is integrated over any section of the flow field and this value is regarded as the reference value [25].

The relative maximum momentum residuals with respect to the three velocity components of u, v, w are

$$\mathrm{Rs}_{U\mathrm{Mom}} = \frac{\mathrm{MAX}\left\{\left|a_e u_e^0 - \left[\sum_{\mathrm{nb}} a_{\mathrm{nb}} u_{\mathrm{nb}}^0 + b + A_e(p_P - p_E)\right]\right|\right\}}{\rho u_m^2} \tag{30}$$

Table 1. Some correspondences between $\alpha_{u,v,w}$ and E

$\alpha_{u,v,w}$	0.1	0.5	0.9	0.95	0.96	0.97	0.98	0.99	1
E	0.111	1	9	19	24	32.3	49	99	infinite

$$\mathrm{Rs}_{V\mathrm{Mom}} = \frac{\mathrm{MAX}\{|a_n v_n^0 - [\sum_{\mathrm{nb}} a_{\mathrm{nb}} v_{\mathrm{nb}}^0 + b + A_n(p_P - p_N)]|\}}{\rho u_m^2} \tag{31}$$

$$\mathrm{Rs}_{W\mathrm{Mom}} = \frac{\mathrm{MAX}\{|a_t w_t^0 - [\sum_{\mathrm{nb}} a_{\mathrm{nb}} w_{\mathrm{nb}}^0 + b + A_t(p_P - p_T)]|\}}{\rho u_m^2} \tag{32}$$

where u^0, v^0, and w^0 are the initial velocities at each iteration level and ρu_m^2 is the reference momentum. For open systems, the inlet momentum is taken as the reference value. For closed systems, the momentum is integrated over any section in the flow field to achieve the reference value [25].

Double-precision computations. Double precision is adopted to reduce the truncation error and numerical noise.

6. NUMERICAL COMPARISONS

Four problems were studied using both the IDEAL+ADI method and the IDEAL+Bi-CGSTAB method:

Problem 1: Laminar flow over a backward-facing step
Problem 2: Laminar flow through a duct with a complicated structure
Problem 3: Lid-driven cavity flow in a cubic cavity
Problem 4: Lid-driven cavity flow in a cubic cavity with a complicated structure

Problems 1 and 2 refer to open systems; Problems 3 and 4 refer to closed systems. The assumptions involved in these problems are: laminar, incompressible, steady-state, and constant physical properties of fluid.

6.1. Problems of Open Systems

Problem 1: Laminar flow over a backward-facing step. The configuration shown in Figure 4 is a simple open system, which has been widely used as a typical configuration in computational fluid dynamics study. The domain extension method [25] is used to deal with the solid step, i.e., the solid step is assumed to be a fluid with sufficiently high viscosity, thus numerical computations are performed over the whole region $2H \times 8H \times 25H$.

Calculations are conducted for $\mathrm{Re} = 100$–300 and grid number $= 127 \times 32 \times 63$. The inflow velocity distribution is cited from Shah and London [31], and the fully developed boundary condition is used at the outflow boundary. The residuals $\mathrm{Rs}_{\mathrm{Mass}}$, $\mathrm{Rs}_{U\mathrm{Mom}}$, $\mathrm{Rs}_{V\mathrm{Mom}}$, and $\mathrm{Rs}_{W\mathrm{Mom}}$ are all set to be less than 10^{-7}. The Reynolds number is defined by

$$\mathrm{Re} = \frac{u_{\mathrm{in}} H}{\nu} \tag{33}$$

Figure 5 shows the reattachment length (i.e., L_R) on plane $z = 4H$, computed by the IDEAL+ADI method and the IDEAL+Bi-CGSTAB method, and cited from [32].

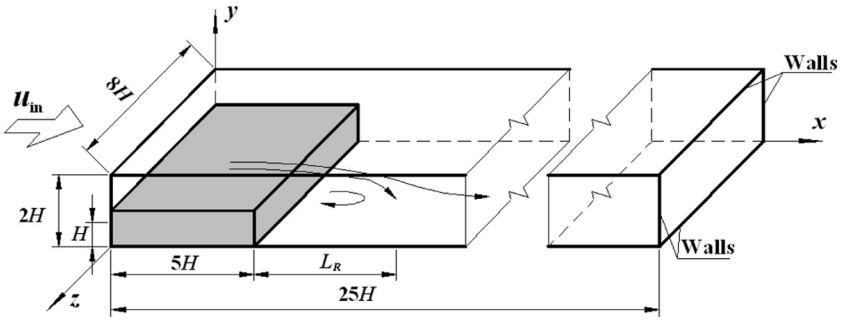

Figure 4. Flow configuration of laminar fluid flow over a backward-facing step.

The two computed results by the IDEAL+ADI method and the IDEAL+Bi-CGSTAB method agree very well with those cited from [32], verifying the reliability of the IDEAL+ADI method, the IDEAL+Bi-CGSTAB method, and the developed code.

Figures 6 and 7 show the computation time and robustness of the IDEAL+ADI and IDEAL+Bi-CGSTAB methods for different Reynolds numbers in Problem 1. The inner iteration times N1 and N2 in the IDEAL algorithm are displayed in these figures. Different N1 and N2 are adopted corresponding to different ranges of time-step multiples. For example, as shown in Figure 6, N1 and N2 of the IDEAL+ADI method for different time-step multiple ranges are 1 and 1, 4 and 4, and 5 and 5, respectively. N1 and N2 of the IDEAL+Bi-CGSTAB method are 1 and 1, 2 and 2, 4 and 4, 6 and 6, 8 and 8, and 12 and 12, respectively.

Four features can be seen from Figures 6 and 7:

1. N1 and N2 are increased with the increase of time-step multiples for the IDEAL+ADI method and the IDEAL+Bi-CGSTAB method.

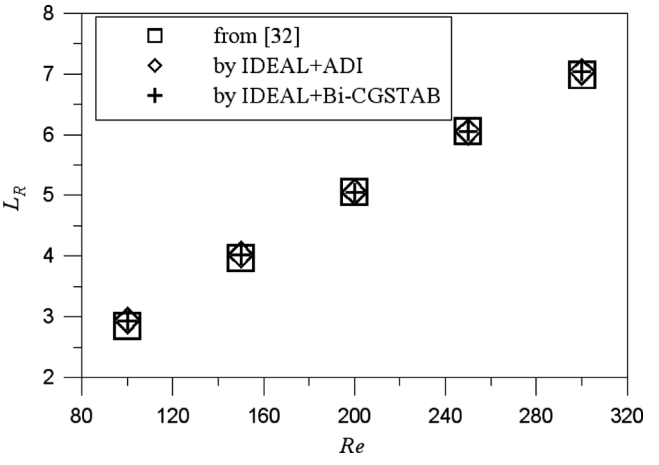

Figure 5. Predicted reattached length L_R on plane $z = 4H$.

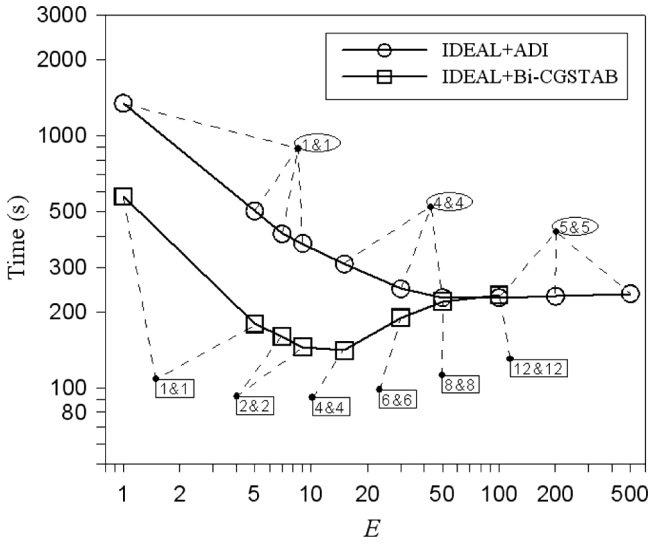

Figure 6. Comparison of computation time and robustness of IDEAL+ADI and IDEAL+Bi-CGSTAB methods for Re = 100 with grid number = $127 \times 32 \times 63$ for Problem 1.

2. The convergence rate of the IDEAL+Bi-CGSTAB method is faster than that of the IDEAL+ADI method for small time-step multiples, but the two methods have nearly the same convergence rates for large time-step multiples.
3. The computation time of the IDEAL+Bi-CGSTAB method is decreased by 38% for Re = 100 and by 27% for Re = 300, over the IDEAL+ADI method.

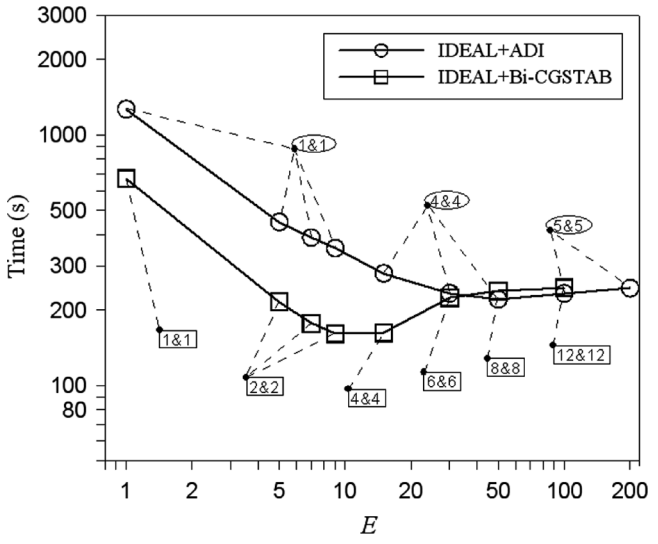

Figure 7. Comparison of computation time and robustness of IDEAL+ADI and IDEAL+Bi-CGSTAB methods for Re = 300 with grid number = $127 \times 32 \times 63$ for Problem 1.

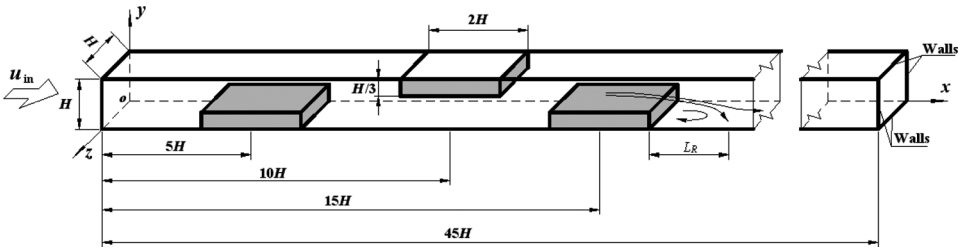

Figure 8. Flow configuration of laminar fluid flow through a duct with complicated structure.

4. The IDEAL+ADI method can be converged over a very wide range of time step multiples, but the IDEAL+Bi-CGSTAB method may not converge at very large time-step multiples, such as $E > 100$. In addition, the IDEAL+Bi-CGSTAB method needs larger iteration times of N1 and N2 than the IDEAL+ADI method to get convergent results.

It is noted that the IDEAL+Bi-CGSTAB method is still more robustess than the SIMPLER+ADI, PISO+ADI, and SIMPLEC+AD methods (see Figure 13 in [13]). On the whole, the IDEAL+Bi-CGSTAB method has better performance than the IDEAL+ADI method for open systems.

Problem 2: Laminar flow through a duct with complicated structure. Problem 2 deals with an intricate open system. Figure 8 shows the flow configuration, with three blocks of baffle plates inserted in the duct. The three solid blocks are treated by the domain extension method.

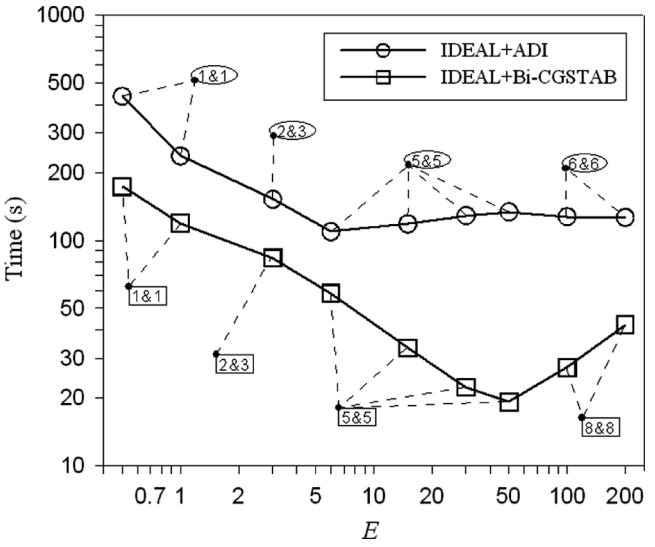

Figure 9. Comparison of computation time and robustness of IDEAL+ADI and IDEAL+Bi-CGSTAB methods for Re = 100 with grid number = $150 \times 20 \times 20$ for Problem 2.

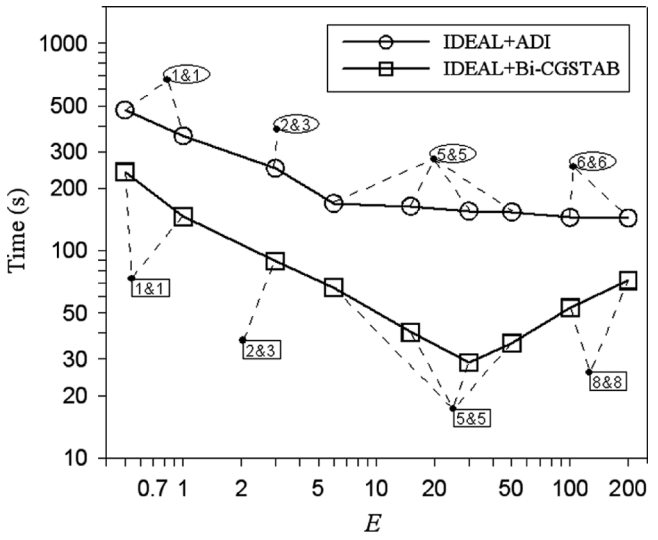

Figure 10. Comparison of computation time and robustness of IDEAL+ADI and IDEAL+Bi-CGSTAB methods for Re = 300 with grid number = $150 \times 20 \times 20$ for Problem 2.

Calculations are conducted for Re = 100–300, grid number = $150 \times 20 \times 20$. The inflow velocity is uniform, and the fully developed boundary condition is used at the outflow. The residuals $\mathrm{Rs}_{\mathrm{Mass}}$, $\mathrm{Rs}_{U\mathrm{Mom}}$, $\mathrm{Rs}_{V\mathrm{Mom}}$, and $\mathrm{Rs}_{W\mathrm{Mom}}$ are set to be less than 10^{-7}. The Reynolds number is defined as

$$\mathrm{Re} = \frac{u_{\mathrm{in}} H}{\nu} \tag{34}$$

Figures 9 and 10 show the computation time versus the time-step multiples for the IDEAL+ADI method and the IDEAL +Bi-CGSTAB method at different Reynolds numbers. It is seen from Figures 9 and 10 that the IDEAL+Bi-CGSTAB method significantly reduces the computation time. The computation time of the IDEAL+BI-CGSTAB method is reduced by 83% at Re = 100 and by 80% at Re = 300, compared with the IDEAL+ADI method. The ranges of time-step multiples that can sustain the convergent solution are nearly the same using the two methods. Both methods are more robust than the SIMPLER+ADI, PISO+ADI, and SIMPLEC+ADI methods (see Figure 16 in [13]).

Incorporating Problem 1, we conclude that the IDEAL+Bi-CGSTAB method has much faster convergence rate than the IDEAL+ADI method. The robustness is nearly the same for both methods, or it is slightly weakened for the IDEAL+Bi-CGSTAB method. Both methods are superior to those that have been reported in the literature.

6.2. Problems of Closed Systems

Problem 3: Lid-driven cavity flow in a cubic cavity. This problem has served as a benchmark CFD/NHT problem to test numerical methods for

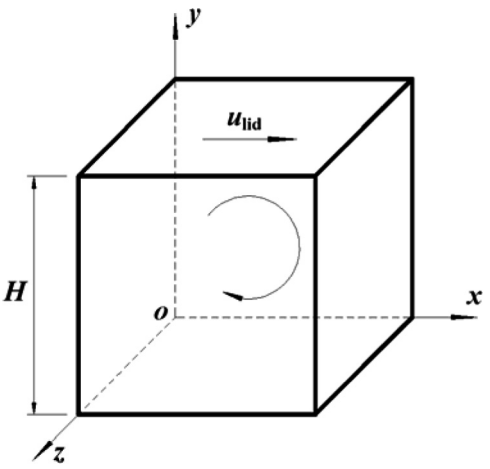

Figure 11. Flow configuration of lid-driven cavity flow in a cubic cavity.

three-dimensional fluid flows [33–35]. Figure 11 shows the flow configuration. Calculations are conducted for Re = 100–1,000 and grid number = $82 \times 82 \times 82$. The residuals of $\mathrm{Rs_{Mass}}$, $\mathrm{Rs}_{U\mathrm{Mom}}$, $\mathrm{Rs}_{V\mathrm{Mom}}$, and $\mathrm{Rs}_{W\mathrm{Mom}}$ are smaller than 10^{-8}. The Reynolds number is defined as

$$\mathrm{Re} = \frac{u_{\mathrm{lid}} H}{\nu} \tag{35}$$

Figure 12 illustrates the velocity profiles along the centerlines on the plane $z = 0.5H$. The velocity profiles computed by both the IDEAL+Bi-CGSTAB method and the IDEAL+ADI method are in excellent agreement with those reported by Tang et al. [35].

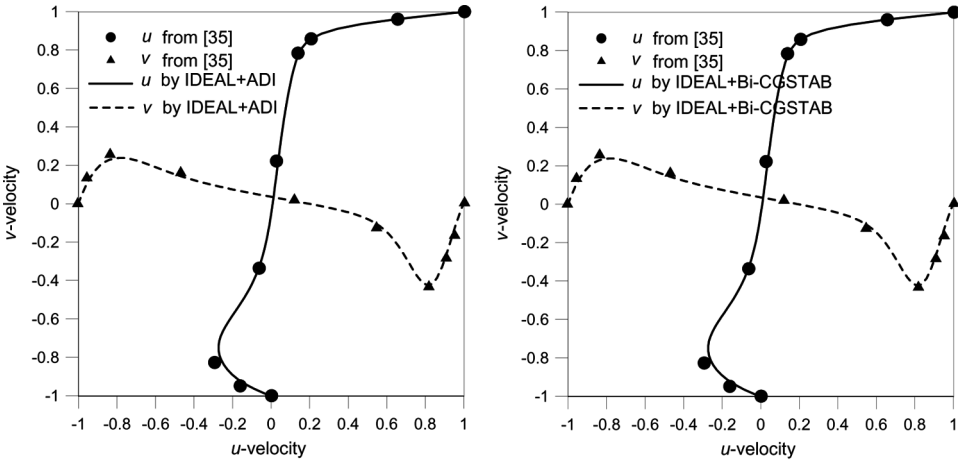

(*a*) IDEAL+ADI method (*b*) IDEAL+Bi-CGSTAB method

Figure 12. Comparison of velocity profiles u and v along the central axes on plane $z = 0.5H$ for Re = 1,000.

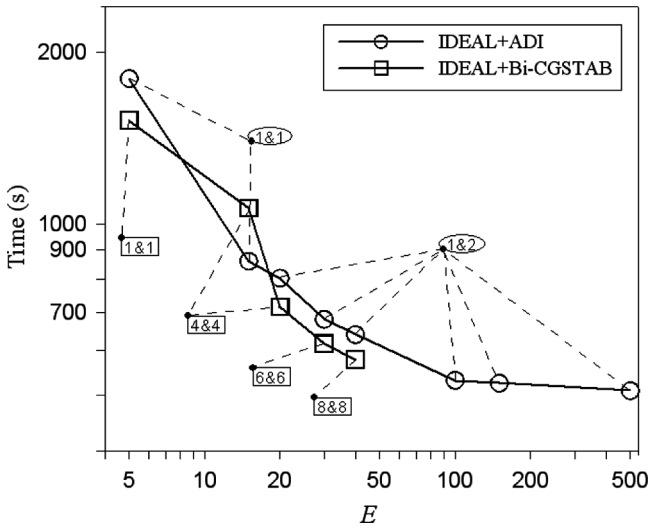

Figure 13. Comparison of computation time and robustness of IDEAL+ADI and IDEAL+Bi-CGSTAB methods for Re = 100 with grid number = $82 \times 82 \times 82$ for Problem 3.

Figures 13 and 14 show the computation time versus the time-step multiple E using the IDEAL+Bi-CGSTAB and IDEAL+ADI methods for different Reynolds numbers. Generally, the difference in computation time using the two methods is not large. The curves of computation time versus time-step multiple are crossed by the two methods, i.e., the computation time of the IDEAL+Bi-CGSTAB method is

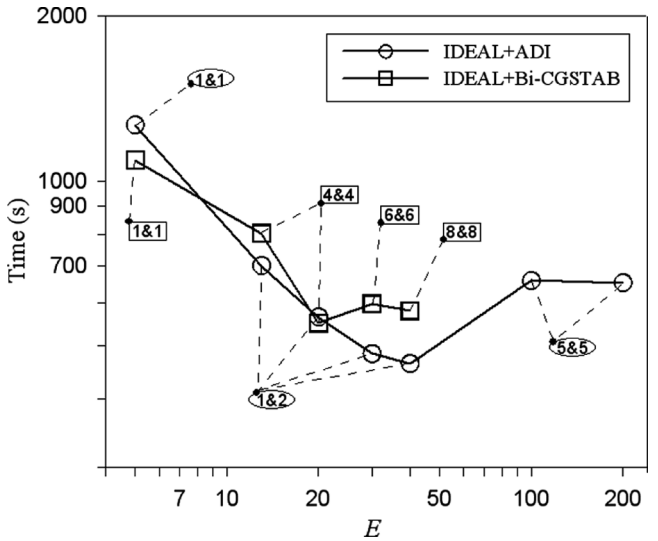

Figure 14. Comparison of computation time and robustness of IDEAL+ADI and IDEAL+Bi-CGSTAB methods for Re = 1,000 with grid number = $82 \times 82 \times 82$ for Problem 3.

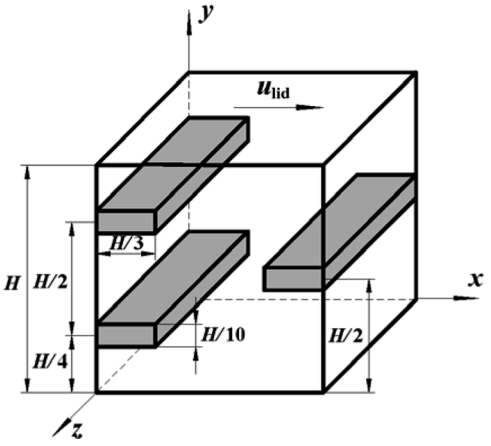

Figure 15. Flow configuration of lid-driven cavity flow in a cubic cavity with complicated structure.

occasionally larger, but occasionally smaller, than that of the IDEAL+ADI method. Another finding is that the range of the time-step multiple is narrowed by IDEAL+Bi-CGSTAB method, showing the weakened robustness of the IDEAL+Bi-CGSTAB method, compared with the IDEAL+ADI method.

Problem 4: Lid-driven cavity flow in a cubic cavity with complicated structure. This problem refers to a complicated closed system. Figure 15 shows the flow configuration, with three blocks of baffle plates inserted in the cubic cavity. Again, the three solid blocks are treated by the domain extension method.

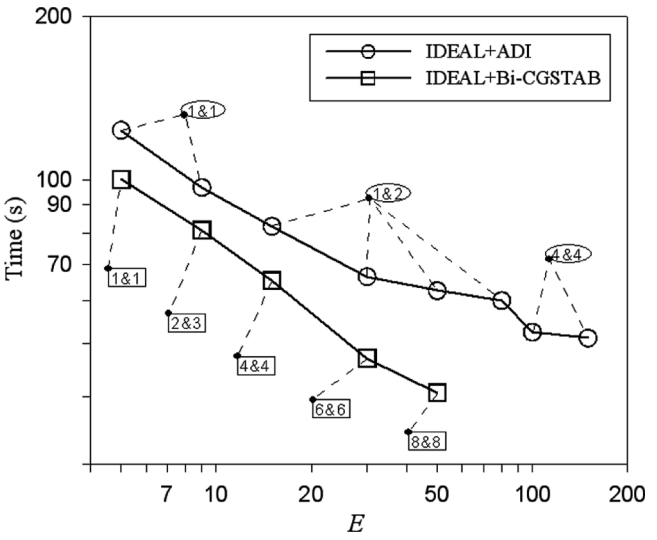

Figure 16. Comparison of computation time and robustness of IDEAL+ADI and IDEAL+Bi-CGSTAB methods for Re = 100 with grid number = $52 \times 52 \times 52$ for Problem 4.

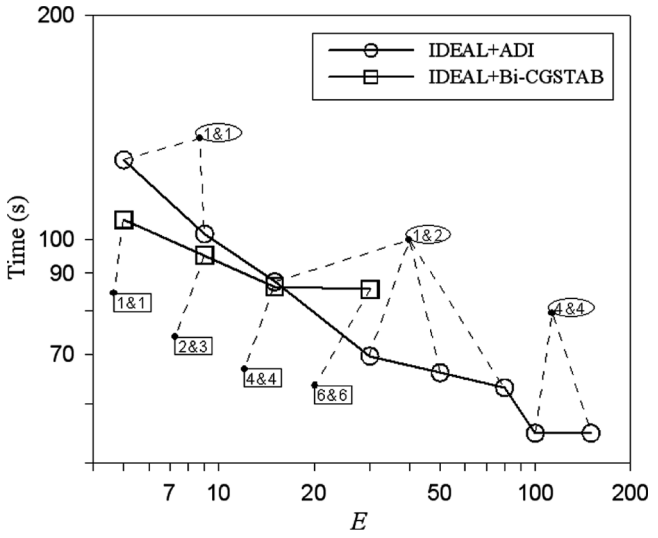

Figure 17. Comparison of computation time and robustness of IDEAL+ADI and IDEAL+Bi-CGSTAB methods for $Re = 500$ with grid number $= 52 \times 52 \times 52$ for Problem 4.

Calculations are conducted for Re = 100–500 and grid number $= 52 \times 52 \times 52$. The residuals $\mathrm{Rs}_{\mathrm{Mass}}$, $\mathrm{Rs}_{U\mathrm{Mom}}$, $\mathrm{Rs}_{V\mathrm{Mom}}$, and $\mathrm{Rs}_{W\mathrm{Mom}}$ are smaller than 10^{-8}. The Reynolds number is defined as

$$\mathrm{Re} = \frac{u_{\mathrm{lid}} H}{\nu} \tag{36}$$

As shown in Figure 16, the IDEAL+Bi-CGSTAB method needs less computation time than the IDEAL+ADI method at Re = 100, but the curves of computation time versus time-step multiple are crossed between the two methods at Re = 500 (see Figure 17). As shown in Figures 16 and 17, the range of the time-step multiple to reach the convergent solution is shortened by the IDEAL+Bi-CGSTAB method, showing the inferior performance of the IDEAL+Bi-CGSTAB method.

7. CONCLUSIONS

In this article, four three-dimensional incompressible fluid flow problems have been examined by the methods of IDEAL+Bi-CGSTAB and IDEAL+ADI. The conclusions are summarized as follows.

1. For open systems, the IDEAL+Bi-CGSTAB method reduces the computation time to reach the convergent solution by 27–83%, compared with the IDEAL+ADI method. The range of the time–step multiple may be slightly narrower for the IDEAL+Bi-CGSTAB than for the IDEAL+ADI method, showing slightly weakened robustness of the IDEAL+Bi-CGSTAB method. Generally,

the IDEAL+Bi-CGSTAB method is better than the IDEAl+ADI method to simulate open systems.

2. For closed systems, depending on the Reynolds number, the curves of computation time versus time-step multiple may be crossed between the two methods, or the IDEAL+Bi-CGSTAB method reduces the computation time, compared with the IDEAL+ADI method. The range of the time-step multiple is narrowed by the IDEAL+Bi-CGSTAB method. In summary, the IDEAL+Bi-CGSTAB method is inferior to the IDEAL+ADI method.

REFERENCES

1. W. Shyy and R. Mittal, Solution Methods for the Incompressible Navier-Stokes Equations, in R. W. Johnson (ed.), *Handbook of Fluid Dynamics*, pp. 31.1–31.33, CRC Press, Boca Raton, FL, 1998.
2. W. Q. Tao, *Recent Advances in Computational Heat Transfer*, Science Press, Beijing, 2000.
3. S. V. Patankar and B. Spalding, A Calculation Procedure for Heat Mass and Momentum Transfer in Three Dimensional Parabolic Flows, *Int. J. Heat Mass Transfer*, vol. 15, pp. 1787–1806, 1972.
4. S. V. Patankar, *Numerical Heat Transfer and Fluid Flow*, Hemisphere, Washington, DC, 1980.
5. S. V. Patankar, A Calculation Procedure for Two-Dimensional Elliptic Situations, *Numer. Heat Transfer*, vol. 4, pp. 409–425, 1981.
6. J. P. Van Doormaal and G. D. Raithby, Enhancements of the SIMPLE Method for Predicting Incompressible Fluid Flows, *Numer. Heat Transfer*, vol. 7, pp. 147–163, 1984.
7. J. P. Van Doormaal and G. D. Raithby, An Evaluation of the Segregated Approach for Predicting Incompressible Fluid Flow, *ASME Paper* 85-HT-9, 1985.
8. R. I. Issa, Solution of Implicitly Discretized Fluid Flow Equation by Operator-Splitting, *J. Comput. Phys.*, vol. 62, pp. 40–65, 1985.
9. W. Q. Tao, Z. G. Qu, and Y. L. He, A Novel Segregated Algorithm for Incompressible Fluid and Heat Transfer Problems—CLEAR (Coupled and Linked Equations Algorithm Revised) Part I: Mathematical Formulation and Solution Procedure, *Numer. Heat Transfer, B*, vol. 45, pp. 1–17, 2004.
10. W. Q. Tao, Z. G. Qu, and Y. L. He, A Novel Segregated Algorithm for Incompressible Fluid and Heat Transfer Problems—CLEAR (Coupled and Linked Equations Algorithm Revised) Part II: Application Examples, *Numer. Heat Transfer B*, vol. 45, pp. 19–48, 2004.
11. D. L. Sun, Z. G. Qu, Y. L. He, and W. Q. Tao, An Efficient Segregated Algorithm for Incompressible Fluid Flow and Heat Transfer Problems—IDEAL (Inner Doubly-Iterative Efficient Algorithm for Linked-Equations) Part I: Mathematical Formulation and Solution Procedure, *Numer. Heat Transfer, B*, vol. 53, pp. 1–17, 2008.
12. D. L. Sun, Z. G. Qu, Y. L. He, and W. Q. Tao, An Efficient Segregated Algorithm for Incompressible Fluid Flow and Heat Transfer Problems—IDEAL (Inner Doubly Iterative Efficient Algorithm for Linked Equations) Part II: Application Examples, *Numer. Heat Transfer, B*, vol. 53, pp. 18–38, 2008.
13. D. L. Sun, Z. G. Qu, Y. L. He, and W. Q. Tao, Performance Analysis of IDEAL Algorithm for Three-Dimensional Incompressible Fluid Flow and Heat Transfer Problems, *Int. J. Numer. Meth. Fluids*, vol. 61, pp. 1132–1160, 2009.
14. D. L. Sun, Z. G. Qu, Y. L. He, and W. Q. Tao, Implementation of an Efficient Segregated Algorithm—IDEAL on a 3D Collocated Grid System, *Chinese Sci. Bull.*, vol. 54, pp. 929–942, 2009.

15. W. F. Ames, *Numerical Methods for Partial Differential Equations*, 2nd ed., Academic Press, New York, 1977.
16. Y. Saad, *Iterative Methods for Sparse linear Systems*, PWS Publishing, New York, 1996.
17. H. A. Van Der Vorst, BI-CGSTAB: A Fast and Smoothly Converging Variant of BI-CG for the Solution of Nonsymmetric Linear Systems, *SIAM J. Sci. Stat Compu.*, vol. 13, pp. 631–644, 1992.
18. H. A. Van Der Vorst, Efficient and Reliable Iterative Methods for Linear Systems, *J. Comput. Appl. Mathe.*, vol. 149, pp. 251–265, 2002.
19. Y. Saad and M. H. Schultz, GMRES: A Generalized Minimal Residual Algorithm for Solving Nonsymmetric Linear Systems, *SIAM J. Sci. Stat. Comput.*, vol. 7, pp. 856–869, 1986.
20. J. B. Zhao and Z. H. Sheng, An Improved Conjugate Gradient Square Algorithm, *J. Southeast Univ. (Nat. Sci. Ed.)*, vol. 29, no. 3, pp. 43–48, 1999.
21. R. W. Freund, A Transpose-Free Quasi-minimal Residual Algorithm for Non-Hermitian Linear Systems, *SIAM J. Sci. Stat. Comput.*, vol. 14, pp. 470–482, 1993.
22. R. W. Freund and N. M. Nachtigal, An Implementation of the QMR Method Based on Coupled Two-Term Recurrences, *SIAM J. Sci. Stat. Comput.*, vol. 15, pp. 313–337, 1994.
23. W. W. Jin, D. L. Sun, and W. Q. Tao, Analysis of Solution Characteristic for Krylove Subspace Methods in SIMPLER Algorithm, *J. Eng. Thermophys.*, vol. 28, pp. 478–480, 2007.
24. S. M. Yang and W. Q. Tao. *Heat Transfer*, 4th, ed., pp. 80–81, Higher Education Press, Beijing, 2006.
25. W. Q. Tao, *Numerical Heat Transfer*, 2nd ed., Xi'an Jiaotong University Press, Xi'an, China, 2001.
26. H. K. Versteeg and W. Malalasekera, *An Introduction to Computational Fluid Dynamics, The Finite Volume Method*, Longman Scientific & Technical, Essex, UK, 1995.
27. I. Gustafsson, A Class of 1st Order Factorization Methods, *BIT*, vol. 18, pp. 142–156, 1978.
28. Z. Y. Li and W. Q. Tao, A New Stability-Guaranteed Second-Order Difference Scheme, *Numer. Heat Transfer B*, vol. 42, pp. 349–365, 2002.
29. P. K. Khosla and S. G. Rubin, A Diagonally Dominant Second Order Accurate Implicit Scheme, *Comput. Fluids*, vol. 2, pp. 207–209, 1974.
30. T. Haysae, J. A. C. Humphery, and A. R. Grief, A Consistently Formulated QUICK Scheme for Fast and Stable Convergence Using Finite Volume Iterative Calculation Procedures, *J. Comput. Phys.*, vol. 93, pp. 108–118, 1992.
31. R. K. Shah and A. L. London, *Laminar Forced Convection in Ducts, Supplements to Advances in Heat Transfer*, Academic Press, New York, 1978.
32. J. H. Nie and B. F. Armaly, Reattachment of Three-Dimensional Flow Adjacent to Backward-Facing Step, *ASME J. Heat Transfer*, vol. 125, pp. 422–428, 2003.
33. H. C. Ku, R. S. Hirsh, and T. D. Taylor, A Pseudospectral Method for Solution of the Three-Dimensional Incompressible Navier-Stokes Equations, *J. Comput. Phys.*, vol. 70, pp. 439–462, 1987.
34. G. Guj and F. Stella, A Vorticity-Velocity Method for the Numerical Solution of 3D Incompressible flows, *J. Compu. Phys.*, vol. 106, pp. 286–298, 1993.
35. L. Q. Tang, T. Cheng, and T. T. H. Tsang, Transient Solutions for Three-Dimensional lid-Driven Cavity Flows by a Least-Squares Finite Element Method, *Int. J. Numer. Meth. Fluids*, vol. 21, pp. 413–432, 1995.